Generation of Pathloss and Interference Maps as SON Enabler in Deployed UMTS Networks

Conference Paper · May 2009

DOI: 10.1109/VETECS.2009.5073570 · Source: IEEE Xplore

2 authors, including:

Christopher Brunner
Qualcomm
36 PUBLICATIONS **661** CITATIONS

SEE PROFILE

Generation of Pathloss and Interference Maps as SON Enabler in Deployed UMTS Networks

Christopher Brunner and Dino Flore
Qualcomm
{Chris.Brunner, Dino.Flore}@qualcomm.com

Abstract—**In modern cellular systems such as HSPA and LTE, link- and cell level performance has largely been optimized. This is less true for performance on inter-cell level where antenna parameters and new site locations are set based on expensive and limited drive tests and inaccurate propagation models. Since the 3G ecosystem already provides devices for data collection at the radio network controller, RF optimization tools, and remotely configurable antennas, the missing component and the focus of this paper is the conversion of collected data into useful input for RF optimization tools. In particular, we propose to position measurement report messages sent from terminals to radio network controller for active set management to generate accurate pathloss, interference, and demand maps. To evaluate if the presented positioning scheme is sufficiently accurate, all antennas of a network are turned in a simulation to obtain the CDFs of errors in predicted antenna gain changes caused by positioning errors. The data indicates that the positioning accuracy is sufficient for 3 sector deployments. To support the deployment of micro- and picocells as well as higher order sectorization, ideas to enhance the positioning scheme are outlined.**

I. INTRODUCTION

Data usage is experiencing strong growth in many 3G networks (USB dongles w/ HSPA modems, advanced smart phones). Since data usage is not homogeneous and potential site locations are limited, differently sized cells on the same carrier are required to provide capacity efficiently. However, smaller cells obtained by micro- and picocell deployments or higher order sectorization are harder to plan for and optimize due to interference and pilot pollution in re-use 1 type networks. This is driving the development of self optimizing networks (SON) in general and capacity and coverage optimization in particular [3]. A few approaches are listed here: With remotely configurable antennas, downtilt and pilot Tx power can be applied on the fly to exploit daily traffic patterns based on accurate path-loss and demand maps. Antenna beam-width optimization can yield ~20% if only one of three sectors is overloaded. With accurate maps, new sites for microcells can be selected where both demand and isolation to neighboring cells are high. High isolation lowers the attenuation applied to the micro-/picocell uplink to mitigate link imbalance. Higher order sectorization is not widely used even though new sites are not required since pilot pollution and large soft handover area are considered difficult to contain. In theory, capacity gains of up to ~80% are possible (3 -> 6 cells/site) if antennas with sharp roll-off are used. With accurate input into optimization tools, gains based on optimal cell antenna configurations can be determined in advance to decide for which sites this deployment makes sense.

The paper is structured as follows: Section 2 covers the positioning of the measurement report messages (MRMs). We did not consider GPS due to limited indoor availability. Instead, we modified Enhanced OTD [6] to jointly estimate MRM positions based on observed time differences (OTDs) reported in the MRMs and relative time differences (RTDs) between cells, Section 2.2. Without RTD estimates, expensive location management units are required in asynchronous networks. MRM positioning is further improved by a locally linear prediction model of successive positions for Kalman filtering, cf. Section 2.3. Results are shown in Section 2.4. Section 3 covers map generation and sensitivity to MRM position error.

II. MRM POSITIONING

A. Input and System Model

Fig. 1 shows 4 input groups: cell configuration, MRM, RTT (round trip time), and elevation data. Operators can provide cell configuration and elevation data. MRM and RTT data can be obtained at radio network controllers or with network probes.

The cell configuration data group consists of site location in WGS84 format and antenna height, pilot power to determine pathloss together with signal strength measurements, and sector number to determine the offset of each cell of a nodeB with respect to its clock, thus reducing unknowns. Furthermore, to map cell measurements reported in MRMs to site locations of cells, the pilot scrambling code (PSC) or the Cell ID of the cell is required. The Cell ID has the advantage over the PSC that it is unique. In UMTS, only 512 PSCs are available to separate cells.

The MRM data group is comprised of MRMs [2] which are configured to report PSC, RSCP (signal strength), Ec/No (signal quality), and OTD for each measured cell [1]. OTDs are used to position the MRMs and path-loss and interference maps are generated with positioned signal strength and quality measurements. Furthermore, the time-stamp and a parameter such as the U-RNTI (layer 3 connection identifier [2])

978-1-4244-2517-4/09/$20.00 ©2009 IEEE

assigning an MRM to a connection is required for motion model based Kalman filtering. If the PSCs can be mapped to Cell~IDs based on proximity, ambiguity with respect to measured cells can be avoided. The OTD between terminal clock and cell clock is measured in chips where one chip corresponds to 0.26us or 78m. In general, MRM reporting is event triggered.

To map RTT measurements to the right connection, an U-RNTI is required. RTT time-stamps allow merging RTT with OTD measurements. Cell IDs rather than PSCs of RTT measurements uniquely determine the measured cell.

Elevation data is provided in WGS84 format to reduce MRM positioning unknowns from 3 to 2.

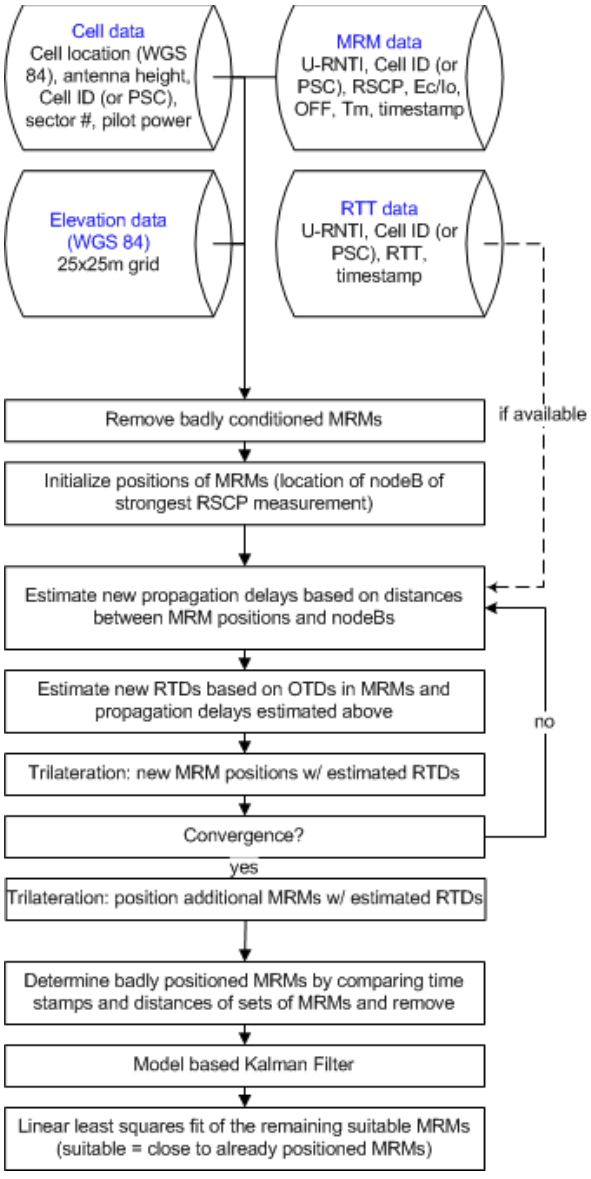

Figure 1: Flow Chart

In the system model, OTDs $T_{\mathrm{OTD},k}(i)$ between i-th nodeB[1] and terminal position reported in the k-th MRM, propagation delays $\tau_k(i)$, terminal clock when k-th MRM is triggered, t_k, and cell clocks $t_{\mathrm{NB}}(i)$ elate to one another as follows:

$$T_{\mathrm{OTD},k}(i) = t_k - (t_{\mathrm{NB}}(i) + \tau_k(i)) \qquad (1)$$

With $T_{\mathrm{RTD}}(i,j) = t_{\mathrm{NB}}(j) - t_{\mathrm{NB}}(i)$ and (1), we obtain

$$T_{\mathrm{RTD}}(i,j) = T_{\mathrm{OTD},k}(i) - T_{\mathrm{OTD},k}(j) - (\tau_k(j) - \tau_k(i)) \qquad (2)$$

$T_{\mathrm{RTD}}(i,j)$ denotes the RTDs between nodeBs i and j. Field tests indicated that the cell clock drift is negligible over a period of two days.

B. OTD Based Iterative Positioning

Before starting the iteration, a subset of MRMs can be selected to accelerate convergence of RTD estimates. The position of each remaining MRM is initialized at the site with the strongest signal strength measurement.

The first iteration step consists of computing propagation delays between nodeB positions $\mathbf{y}_{\mathrm{NB}}(i)$ and estimates of MRM positions

$$\tau_k(i) = \| \mathbf{y}_{\mathrm{NB}}(i) - \mathbf{y}_k \| / c \qquad (3)$$

where c denotes speed of light and $\mathbf{y}_k$ the position of the k-th MRM. If available, RTT measurements[2] can replace estimates of $\tau_k(i)$ as indicated in the flow chart shown in Fig. 1.

The second iteration step consists of computing RTDs based on OTDs and propagation delays estimated in (3). Every MRM m measuring the two sites i and j provides an RTD sample (2). The following vector contains all samples pairs of sites,

$$\mathbf{T}_{\mathrm{RTD}}(i,j) = (\ldots T_{\mathrm{RTD}}(i,j,m) \ldots)^{\mathrm{T}}$$

Instead of computing the median of $\mathbf{T}_{\mathrm{RTD}}(i,j)$ to obtain the new estimate $T^{+}_{\mathrm{RTD}}(i,j)$, we propose to consider the numbers after the breakpoint in addition to attenuating outliers:

$$T^{+}_{\mathrm{RTD}}(i,j) = \mathrm{mean}(\,\mathrm{sign}(\mathbf{c}^{(i,j)})\ |\mathbf{c}^{(i,j)}|^{p}\,) + \mathrm{median}\,(\,\mathbf{T}_{\mathrm{RTD}}(i,j)\,) \bmod (256 * 38400) \qquad (4)$$

where

$$\mathbf{d}^{(i,j)} = \mathbf{T}_{\mathrm{RTD}}(i,j) - \mathrm{median}\,(\,\mathbf{T}_{\mathrm{RTD}}(i,j)\,)$$

and

$$\mathbf{c}^{(i,j)} = (\mathbf{d}^{(i,j)} + 128 * 38400) \bmod (256 * 38400) - 128 * 38400$$

---

[1] Cells of nodeBs have fixed offsets but for notational simplicity, this is not captured in the notation.

[2] The resolution of the RTT measurements is 1/16 chip or 4.88m, i.e., significantly higher than OTD resolution of 1 chip. On the other hand, RTT measurements are available only for active set links, whereas OTD is measured across active, neighbor, and detected set cells. Furthermore, RTT measurements include a time offset between which the terminal receives and transmits. This time offset is known only for the primary link and corresponds to 1024 chips. Without increasing traffic over the air, the time offset for the non-primary links is unknown.

Here $.^p$ denotes element wise exponentiation. Note that the RTD ranges from 0 to 256* 38400 - 1.

The third iteration step consists of estimating new MRM positions by means of trilateration. With estimated RTDs, cf. (4), and measured OTDs, the relative distance between two sites can be computed as follows:

$$r_k(i,j) = c\,(T_{OTD,k}(i) - T_{OTD,k}(j) - T^{+}_{RTD}(i,j)) \qquad (5)$$

To obtain the k-th MRM position $\mathbf{y}^{+}_k$ for this iteration, the following k-th cost function is minimized

$$\rho_k = \| \begin{pmatrix} r_k(1,2) - d_k(1,2) \\ r_k(1,3) - d_k(1,3) \\ \vdots \\ r_k(i,j) - d_k(i,j) \\ \vdots \end{pmatrix} \| \qquad (6)$$

where

$$d_k(i,j) = \| \mathbf{y}_{NB}(i) - \mathbf{y}_k \| - \| \mathbf{y}_{NB}(k) - \mathbf{y}_k \|$$

holds. Here, $d_k^{(i,j)}$ denotes the relative distance between the i-th and j-th site as a function of $\mathbf{y}_k$. To provide a unique solution, the MRM has to measure at least 3 sites.

Multipath is partially taken into account by only using RTD samples of the strongest cell of a site in (4) and (6).

When the cost function median is not lower than the median 10 iterations ago, convergence of $T_{RTD}(i,j)$ is assumed. Then previously excluded badly conditioned MRMs are positioned with (5) and (6).

C. Motion Model Based Kalman Filter

Since consecutive MRMs are often reported at a frequency higher than 1/s, there is a continuous stream of MRMs tied together by constraints on velocity and acceleration. This motivates the use of a motion model that uses a Kalman filter to fuse position predicted by the motion model with MRM position provided by trilateration. If their time stamps imply unrealistic velocities, MRMs are removed from the set to improve the error distribution, cf. Fig. 1. The motion model is defined in 2-D [5, 7],

$$\mathbf{X}(t_{l+1}) = \mathbf{\Phi}\,\mathbf{X}(t_l) + \mathbf{\Gamma}\,\mathbf{W}(t_l) \qquad (7)$$

where the state vector $\mathbf{X}(t_l)$ denotes location and velocity of the terminal

$$\mathbf{X}(t) = (\,\mathbf{x}(t)\ \mathbf{v}(t)\,)^T$$

and $\mathbf{\Gamma}$ and the state transition matrix $\mathbf{\Phi}$ correspond to

$$\mathbf{\Phi} = \begin{pmatrix} 1 & 0 & \Delta t & 0 \\ 0 & 1 & 0 & \Delta t \\ 0 & 0 & 1 & 0 \\ 0 & 0 & 0 & 1 \end{pmatrix}, \qquad \mathbf{\Gamma} = \begin{pmatrix} 0 & 0 \\ 0 & 0 \\ \Delta t & 0 \\ 0 & \Delta t \end{pmatrix}$$

Furthermore, $\mathbf{W}(t)$ are stochastically independent random errors, normally distributed with expectation $\mathbf{0}$ and covariance matrix $\mathbf{Q} = \sigma^2\,\mathbf{I}_2$. Here, Δt has to be adapted to the inter-arrival times of consecutive event triggered MRMs. Let $\mathbf{X}^{+} = \mathbf{X}(t_0)$ and $\mathbf{C}^{+} = \mathbf{C}(t_0)$. The recursive algorithm is given below:

$$\begin{aligned} &\mathbf{C} = \mathbf{C}^{+} \\ &\mathbf{X} = \mathbf{X}^{+} \\ &\mathbf{C'} = \mathbf{\Phi}\,\mathbf{C}\,\mathbf{\Phi}^{H} \\ &\mathbf{K} = \mathbf{C'}\,\mathbf{M}^{H}\,(\mathbf{M}\ \ \mathbf{C'}\,\mathbf{M}^{H} + \mathbf{R})^{-1} \\ &\mathbf{C}^{+} = \mathbf{C'} - \mathbf{K}\,\mathbf{M}\,\mathbf{C'} \\ &\mathbf{X}^{+} = \mathbf{\Phi}\,\mathbf{X} + \mathbf{K}\,(\mathbf{y}_k - \mathbf{M}\,\mathbf{\Phi}\,\mathbf{X}) \end{aligned} \qquad (8)$$

where

$$\mathbf{M} = \begin{pmatrix} 1 & 0 & 0 & 0 \\ 0 & 1 & 0 & 0 \end{pmatrix}$$

and the measurement vector $\mathbf{y}_k$ denotes the position estimate of the k-th MRM obtained in (6) in x and y. The z-axis value is simply retained.

As initial value for the covariance matrix $\mathbf{C}(t_0)$, we use

$$\mathbf{C}(t_0) = \begin{pmatrix} R & 0 \\ 0 & 30^2 I \end{pmatrix}$$

where $\mathbf{R} = 25000 * \mathbf{I}_2$. 25000 corresponds to a standard deviation of 158m between true and trilaterated position. $30^2(m/s)^2$ is an upper bound for the variance of the initial velocity of the terminal. Initially, $\mathbf{X}(t_0)$ is set to zero velocity and first position estimate obtained in (6).

The filter is also run in reverse to improve positioning accuracy of the initial MRMs of each burst. Finally, previously not considered MRMs that are close in time to already positioned MRMs are positioned by interpolation.

D. MRM Positioning Results

To prove the concept, MRMs were logged from a terminal in connected mode. Test driving took place in a suburban area of 5km*5km. To compute position error, GPS data was collected in parallel. Site distance of the commercial UMTS network varied from 1 to 4km. Elevation data was provided in 25m*25m resolution. The exponent that determines attenuation of outlier RTD samples in (4) was set to p = 0.25. RTT measurements were not available. While only logs from terminals in motion were collected, distributions of position accuracy before Kalman filtering corresponds to accuracy of stationary terminals and are generated in addition to distributions after Kalman filtering. Motion model based Kalman filtering cannot improve position estimates from stationary terminals as successive estimates are correlated. Since MRMs were collected from only one terminal, the number of MRMs measuring several pairs of sites was low. The resulting inaccuracy in RTD estimation introduces a bias in consecutive MRM position estimates. Hence, distributions of

position accuracies are generated based on estimated RTDs[3] as well on 'known' RTDs computed with propagations delays obtained from terminal GPS measurements, cf. (2).

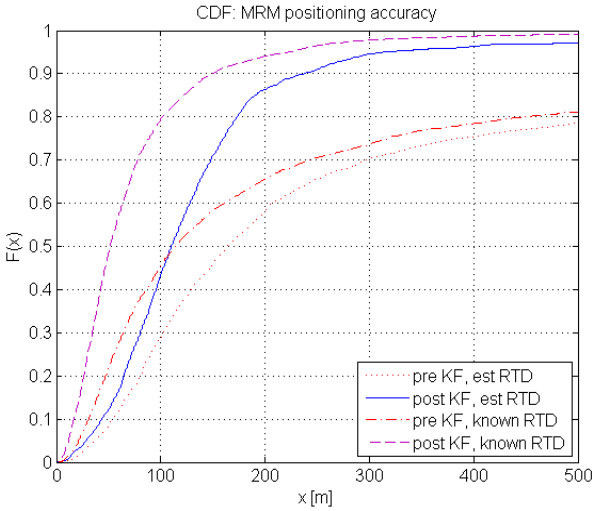

Figure 2: Pre- and post Kalman filter MRM position accuracy based on estimated and 'known' RTDs

Fig. 2 shows the distributions of the position accuracy. The median accuracy before Kalman filtering is 160m for 60.3% (110m for 60.2%) of all MRMs if RTDs are estimated (known). Post Kalman filter, the median accuracy improves to 110m for 58.2% (50m for 58.3%) of all MRMs if RTDs are estimated (known). Note that not all of the badly conditioned MRMs that are discarded initially are positioned. Also see Table 1 for the distribution of number of measured nodeBs. Comparing these numbers with previous work is not trivial because different networks were used. In [8], a pilot correlation method yields mean positioning errors of 75m for urban and 524m for suburban. In [4], a pilot correlation method is proposed as well as a RTT based method. A limitation of the RTT based method is that RTT reporting is limited to active set links and requires additional signaling for non-primary links [1]. The pilot correlation method achieves a median positioning error of about 60m for urban and 120m for suburban.

Table 1: Number of measured nodeBs per MRM. Active set cells, neighbor and detected set cells are measured.

1	2	3	4	5	6	7
8.1%	31.6%	32%	15.9%	9.9%	2.4%	0.1%

Fig. 4 shows positioned MRMs in a section of the test area for 'known' RTDs. Motion model based Kalman filtering of trilateration positions works well if successive MRMs are available and the velocity is non-zero in areas affected by multi-path. Otherwise, consecutive position estimates are affected by the same multi-path, and the position estimate errors are correlated, preventing the Kalman filter from correcting. E.g., in top left of Fig. 4 estimates veer off at a red traffic light.

[3] In case of estimating RTDs, only MRMs with measurements to 4 and more nodeBs are selected. After achieving convergence after 250 iterations, all MRMs with measurements to 3 and more nodeBs are positioned by trilateration based on the previously estimated RTDs. In case of known RTDs, only one iteration is necessary and MRMs with measurements to 3 or more nodeBs are selected.

III. MAP GENERATION AND ACCURACY

Pathloss and interference maps can be generated with positioned pilot strength measurements, known pilot transmit power, and positioned pilot quality measurements. In addition to pathloss maps, RF optimization tools require demand maps which can be generated by logging connection start and stop and applying standard traffic models for voice and data along the positioned route. Since MRMs are event and not periodically triggered, maps will be not accurate in the vicinity towers. For traffic modeling, positions of terminals in dominant coverage of one tower can be estimated by e.g. processing access measurements. On the other hand, it is assumed that position inaccuracies of terminals close to sites have limited impact on cell parameter configuration since little power is needed to serve them.

To evaluate the sensitivity to position errors, 10^{o} in azimuth are added to each antenna in the network. The change in antenna gain for all cells measured by all MRMs positioned with GPS is compared with the error in change due to the MRM position error of Fig. 3. Antenna beamwidths of 65^{o} and 33^{o} are used for 3 and 6 sector deployments.

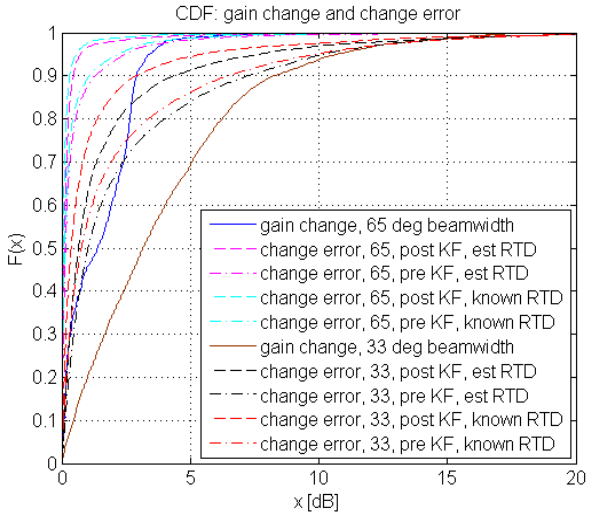

Figure 3: Change in antenna gain after turning all antennas by 10^{o}, error in gain change due to MRM positioning error

For 3 sectors, the post Kalman Filter (KF) and known RTD distribution is the most accurate. Only 2% of the samples have a gain change error larger than 1dB. Note that if the antenna gain for one terminal was not modified as intended due to MRM position error, capacity savings from many other terminals are available to compensate. Close to 90% of the samples with an error larger than 5dB have an antenna gain of less than -20dB. When computing antenna gains, line of sight (LOS) is assumed. It is likely that most of these samples are

caused by reflections happening close to the cell antenna. Then LOS based angle of arrival may not correspond with the main lobe, causing antenna gains to vary significantly with minor errors in position. The 3 sector distribution corresponding to pre-KF (stationary terminals) and estimated RTDs is the worst. Here, 12% of the samples have a gain change error larger than 1dB and 40% of the samples with a gain change error larger than 5dB have an absolute antenna gain of less than -20dB. The degradation is mostly due to the loss in accuracy from not using motion model based KF. The position accuracy seems acceptable.

For 6 sectors, post KF and known RTD, 25% of the samples have a gain change error larger than 1dB. In the pre-KF (stationary terminals) and estimated RTDs combination, 50% of the samples have a gain change error larger than 1dB. Only 28% of the samples with a gain change error larger than 5dB have an absolute antenna gain of less than -20dB. Here, the change error CDF is not significantly smaller than the gain change CDF.

IV. Conclusion and Outlook

We outlined a cost-effective approach to generate RF maps in deployed UMTS systems to increase capacity and coverage. The position accuracy seems acceptable for 3 sector deployments but for higher order sector and microcell deployments, an improved accuracy would be desirable. The following improvements can be considered:

- Tight integration of trilateration with motion model based Kalman filtering.
- Estimation of the offset between terminal clock and site clocks based on already positioned MRMs to allow for time of arrival as opposed to time difference of arrival based positioning.
- Improvement of positioning accuracy at low velocity affected by multipath by storing and utilizing positions matching those OTDs estimated at high velocities.

References

[1] "Third Generation Partnership Project (3GPP), 3G TS 25.215: Physical layer - Measurements (FDD)", www.3gpp.org

[2] "Third Generation Partnership Project (3GPP), 3G TS 25.331: Radio Resource Control (RRC)", www.3gpp.org

[3] "NGNM requirements on SON and OA&M requirements" , July 2008, compiled by NGMN project 12: Self-Organizing Networks.

[4] J. Borkowski and J. Lempiainen, "Practical network-based techniques for mobile positioning in UMTS", in EURASIP Journal on Applied Signal Processing, 2006.

[5] D. Cathrein, M. Hellebrandt, R. Mathar, and M. P. Serrano, "Location tracking of mobiles: A smart filtering method and its use in practice", in IEEE VTC 2004-Spring, 2004.

[6] Timo Halonen, Javier Romero, Juan Melero, "GSM, GPRS and EDGE Performance: Evolution Toward 3G/UMTS", 2003, John Wiley & Sons.

[7] M. Hellebrandt and R. Mathar, "Location tracking of mobiles in cellular networks", in IEEE Transactions on Vehicular Technology, vol. 042, Sept. 1999.

[8] D. Zimmermann, J. Baumann, M. Layh, F. Landstorfer, R. Hoppe, and G. Woelfle, "Database correlation for positioning of mobile terminals in cellular networks using wave propagation models", in IEEE VTC 2004-Fall, 2004.

Figure 4: Raised points show MRM positions estimated using known RTDs. The legend maps raised colors to position accuracy. Ground points are GPS positions of MRMs. Ground colors map to # of measured sites (violett=3, light blue=7).